
DIFFRNN: DIFFERENTIAL VERIFICATION OF RECURRENT NEURAL NETWORKS

A PREPRINT

Sara Mohammadinejad
University of Southern California
saramoha@usc.edu

Brandon Paulsen
University of Southern California
bpaulsen@usc.edu

Chao Wang
University of Southern California
wang626@usc.edu

Jyotirmoy V. Deshmukh
University of Southern California
jdeshmuk@usc.edu

July 21, 2020

ABSTRACT

Recurrent neural networks (RNNs) such as Long Short Term Memory (LSTM) networks have become popular in a variety of applications such as image processing, data classification, speech recognition, and as controllers in autonomous systems. In practical settings, there is often a need to deploy such RNNs on resource-constrained platforms such as mobile phones or embedded devices. As the memory footprint and energy consumption of such components become a bottleneck, there is interest in compressing and optimizing such networks using a range of heuristic techniques. However, these techniques do not guarantee the safety of the optimized network, e.g., against adversarial inputs, or equivalence of the optimized and original networks. To address this problem, we propose DIFFRNN, the first differential verification method for RNNs to certify the equivalence of two structurally similar neural networks. Existing work on differential verification for *ReLU*-based feed-forward neural networks does not apply to RNNs where nonlinear activation functions such as *Sigmoid* and *Tanh* cannot be avoided. RNNs also pose unique challenges such as handling sequential inputs, complex feedback structures, and interactions between the gates and states. In DIFFRNN, we overcome these challenges by bounding nonlinear activation functions with linear constraints and then solving constrained optimization problems to compute tight bounding boxes on non-linear surfaces in a high-dimensional space. The soundness of these bounding boxes is then proved using the *dReal* SMT solver. We demonstrate the practical efficacy of our technique on a variety of benchmarks and show that DIFFRNN outperforms state-of-the-art RNN verification tools such as POPQORN.

1 Introduction

Deep neural networks, and in particular, recurrent neural networks (RNNs), have been successfully used in a wide range of applications including image classification, speech recognition, and natural language processing. However, their rapid growth in safety-critical applications such as autonomous driving [1] and aircraft collision avoidance [2] is accompanied by safety concerns [3]. For example, neural networks are known to be vulnerable to adversarial inputs [4, 5], which are security exploits designed to fool the neural networks [6–9].

In addition, trained neural networks typically go through changes before deployment, thus raising concerns that the changes may introduce new behaviors. Specifically, since neural networks are computationally and memory intense, they are difficult to deploy on resource-constrained devices [10, 11]. Network compression techniques (such as edge pruning, weight quantization, and neuron removal) are often needed to reduce the network’s size [11]. Compression techniques typically use mean-squared error over sampled inputs as a performance measure to test equivalence. Such a measure is statistical, and does not provide formal worst-case guarantees on the deviation between behaviors of two networks.

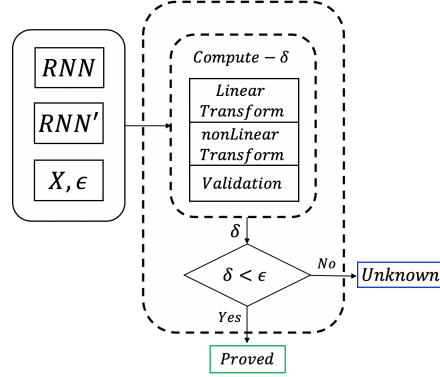


Figure 1: The differential verification flow of DIFFRNN. δ is the difference interval, and ϵ is the bound on the output differences of the compressed and original networks.

While there are recent efforts on applying differential testing [12–14] and fuzzing [15–17] techniques to neural networks, they can only increase the confidence that the networks behave as expected for some of the inputs. However, they cannot prove the equivalence of the networks for all inputs. To the best of our knowledge, RELUDIFF [18] is the only tool that aims to prove the equivalence of two neural networks for all inputs. RELUDIFF takes as input two feed-forward neural networks with piecewise linear activation functions known as rectified linear units (*ReLU*). The *ReLU* activation essentially allows the neural network to be treated as a piecewise linear (PWL) function (with possibly many facets/pieces).

RELUDIFF exploits the PWL nature of activations, and hence cannot natively handle non-PWL activation functions like *Sigmoid*, *Tanh*, and *ELU*, let alone the more complex operations of LSTMs, which take the *product* of these non-linear functions, e.g. *Sigmoid* \times *Tanh*. This poses significant limitations because popular libraries “hardcode” *Tanh* and *Sigmoid* for some, or all of the activation functions in the network. For example, Fig. 3 shows the LSTM structure hardcoded into Tensorflow. Thus, for RNNs, we need a technique that can handle these challenging and arbitrary nonlinearities. In addition, we face several other unique challenges when considering RNNs, including how to *soundly and efficiently* handle (1) sequential inputs, (2) the complex feedback structures, and (3) interactions between the gates and states.

To overcome these challenges, we propose DIFFRNN, the first differential verification technique for bounding the difference of two structurally similar RNNs. Formally, given two RNNs that only differ in numerical values of their edge weights, denoted $\mathbf{y} = f(\mathbf{x})$ and $\mathbf{y}' = f'(\mathbf{x})$, where $\mathbf{x} \in X$ is an input, X is an input region of interest, and \mathbf{y}, \mathbf{y}' are the outputs, DIFFRNN aims to prove that $\forall \mathbf{x} \in X \cdot |f'(\mathbf{x}) - f(\mathbf{x})| < \epsilon$, where ϵ is a reasonably small number.

Fig. 1 shows the high-level flow of DIFFRNN, whose input consists of two networks, *RNN* and *RNN'*, an input region, X , and a small difference bound ϵ . It produces two possible outcomes: *Proved*, or *Unknown*. Internally, DIFFRNN uses symbolic interval arithmetic to compute linear bounds on both the output values of each network’s neurons and the *differences* between the neurons of the two networks. We compute these linear bounds *efficiently* in a layer-by-layer fashion, that is, using the bounds of the previous layer to compute the bounds of the current layer. If the bounds on the final output difference satisfy ϵ , DIFFRNN returns *Proved*, otherwise it returns *Unknown*.

To compute the output difference *accurately*, we bound nonlinear activation functions with linear constraints and then solve constrained optimization problems to obtain tight bounding boxes on nonlinear surfaces in a high-dimensional space. We also prove the soundness of these bounding boxes using *dReal* [19], which is an off-the-shelf *delta-sat* SMT solver¹ that supports nonlinear constraints.

While one could try and adapt an existing single-network verification tool to solve our problem, in practice, the bounds computed by this approach are too loose, since existing tools are not designed to exploit the relationships between neurons in two RNNs. To confirm this observation, we constructed the following experiment. We took two *identical* networks $f(\mathbf{x})$ and $f'(\mathbf{x})$, i.e., with the same network topology and edge weights. We then constructed a new network $f''(\mathbf{x}) = f'(\mathbf{x}) - f(\mathbf{x})$, illustrated in Fig. 2. Then, we took POPQORN, a state-of-the-art RNN verification tool, and attempted to prove $f''(\mathbf{x}) < \epsilon$ for all \mathbf{x} . While POPQORN could not prove this for any $\epsilon < 2.0$, DIFFRNN could prove it easily for any $\epsilon > 0$.

We have implemented our proposed method and evaluated it on a variety of differential verification tasks involving networks for handwritten digit recognition (MNIST) [20] and human activity recognition [21]. Our results show that DIFFRNN is efficient and effective in certifying the functional equivalence of RNNs after compression techniques are

¹*dReal* is implemented based on delta-complete decision procedures; it returns either unsat or delta-sat on the given input formulas, where delta is a user-defined error bound [19].

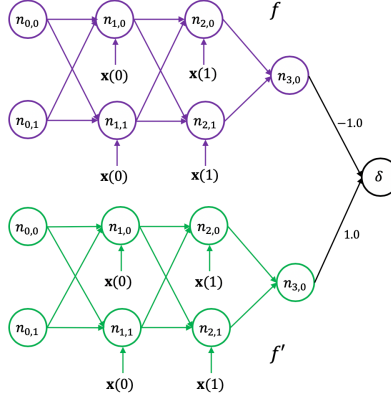


Figure 2: Naïve differential verification of RNNs.

applied. We also compared DIFFRNN with POPQORN [22], the state-of-the-art RNN verification tool. Our results show that DIFFRNN significantly outperforms POPQORN [22]: On average DIFFRNN is 2.73X more accurate and 60% faster.

To summarize, our main contributions are as follows:

- We propose DIFFRNN, a differential verification method for proving the functional equivalence of two structurally similar RNNs.
- We develop techniques to handle the recursive nature of RNNs and nonlinear functions such as *Sigmoid* and *Tanh*.
- We develop techniques to handle both Vanilla RNNs and the more complex LSTMs.
- We formally verify the soundness of our linear approximation techniques using *dReal* [19].
- We experimentally demonstrate that our method significantly outperforms the state-of-the-art techniques.

2 Background

In this section, we review the basics of recurrent neural networks (RNNs), including Vanilla RNNs and LSTMs², and interval bound propagation (IBP), a technique for bounding the network’s output values for all input values.

2.1 Recurrent Neural Networks

2.1.1 Vanilla RNNs

A vanilla recurrent neural network is a function that maps time-indexed *input sequences* to *output sequences*. Let X be a compact subset of \mathbb{R}^m , where m is the number of input values at each time step. An input sequence \mathbf{x} is a function from time $\{0, 1, \dots, T\}$ to input space X , where $T \in \mathbb{N}$, and $\mathbf{x}(j) \in X$ denotes the j^{th} entry in the time-indexed input sequence. An output sequence is a similar function that maps to an output space $Y \subseteq \mathbb{R}^p$.

The structure of a vanilla RNN is as follows. It consists of a single layer of ℓ neurons, and its output \mathbf{h} at time t depends on (a) the output \mathbf{h} at time $t - 1$, and (b) the input \mathbf{x} at time t , as shown below:

$$\mathbf{a}(t) = W_{\mathbf{hh}} \cdot \mathbf{h}(t - 1) + W_{\mathbf{hx}} \cdot \mathbf{x}(t) + \mathbf{b}_{\mathbf{h}} \quad (1)$$

$$\mathbf{h}(t) = \sigma(\mathbf{a}(t)) \quad (2)$$

$$\mathbf{y}(t) = W_{\mathbf{hy}} \cdot \mathbf{h}(t) + \mathbf{b}_{\mathbf{y}} \quad (3)$$

Here, $\mathbf{a}(t)$ is an intermediate variable that we introduce to represent the affine transformation of the current input $\mathbf{x}(t)$ and previous state $\mathbf{h}(t - 1)$. The weight matrices $W_{\mathbf{hh}}$ and $W_{\mathbf{hx}}$ have dimensions $\ell \times \ell$ and $\ell \times m$ respectively. The bias term $\mathbf{b}_{\mathbf{h}}$ is an $\ell \times 1$ matrix. σ is the nonlinear component-wise *activation function* from \mathbb{R}^ℓ to \mathbb{R}^ℓ . We assume that $\mathbf{h}(0)$ is a fixed initial state of the RNN at time 0; it is a vector of size $\ell \times 1$. Finally, the output of the RNN at time t , $\mathbf{y}(t)$ is defined as a linear transformation of $\mathbf{h}(t)$, using the weight matrix $W_{\mathbf{hy}}$ and bias term $\mathbf{b}_{\mathbf{y}}$.

²Gated recurrent units (GRUs) are structurally very similar to LSTMs, and differential verification hurdles for GRUs are the same as LSTMs; thus, we omit explaining GRUs in this paper for brevity.

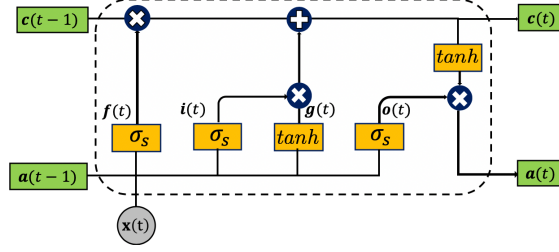


Figure 3: An LSTM cell.

Thus, each multiplication above is a matrix multiplication, and for all time steps t , $\mathbf{h}(t)$ and $\mathbf{x}(t)$ are ℓ - and m -length vectors, respectively. The activation function σ may be the sigmoid activation (σ_S) or the hyperbolic tangent activation (\tanh)³.

In differential verification, there is a second RNN whose parameters are denoted by \mathbf{a}' , \mathbf{h}' , \mathbf{y}' , W'_{hh} , W'_{hx} , W'_{hy} , \mathbf{b}'_{h} and \mathbf{b}'_{y} respectively. The two RNNs under comparison are *structurally similar*, i.e., they only differ in the values of the edge weights, and have the same activation functions.

We also introduce $\delta^{\mathbf{a}}$, $\delta^{\mathbf{h}}$, and $\delta^{\mathbf{y}}$ to represent the differences: $\delta^{\mathbf{a}}(t) = \mathbf{a}'(t) - \mathbf{a}(t)$, $\delta^{\mathbf{h}}(t) = \mathbf{h}'(t) - \mathbf{h}(t)$, and $\delta^{\mathbf{y}}(t) = \mathbf{y}'(t) - \mathbf{y}(t)$.

A many-to-one vanilla RNN differs from the vanilla RNN model shown above in one small way. For an input sequence of length T , the output is computed only at time T , i.e., the final output of the network is defined as $\mathbf{y}(T)$ (see Fig. 6 in Appendix).

2.1.2 LSTMs

Long short-term memory networks (LSTMs) were introduced to overcome the limitation of Vanilla RNNs in learning long term sequential dependencies [23]. Therefore, an LSTM is a special kind of RNN, where each LSTM cell has four neurons that interact with each other. As shown in Fig. 3, each LSTM cell at time step t takes $\mathbf{c}(t-1)$, $\mathbf{h}(t-1)$ and $\mathbf{x}(t)$ as input, and returns $\mathbf{c}(t)$ and $\mathbf{h}(t)$ as output. The input $\mathbf{x}(t)$, the cell state $\mathbf{c}(t)$, and the hidden state $\mathbf{h}(t)$ are all vectors of real values. Thus, the four *gates* and two *states* within each LSTM cell are evaluated as follows:

$$\begin{aligned}
\text{Input gate : } \mathbf{i}(t) &= \sigma_S(W_{\text{ih}} \cdot \mathbf{h}(t-1) + W_{\text{ix}} \cdot \mathbf{x}(t) + \mathbf{b}_{\text{i}}) \\
\text{Forget gate : } \mathbf{f}(t) &= \sigma_S(W_{\text{fh}} \cdot \mathbf{h}(t-1) + W_{\text{fx}} \cdot \mathbf{x}(t) + \mathbf{b}_{\text{f}}) \\
\text{Cell gate : } \mathbf{g}(t) &= \tanh(W_{\text{gh}} \cdot \mathbf{h}(t-1) + W_{\text{gx}} \cdot \mathbf{x}(t) + \mathbf{b}_{\text{g}}) \\
\text{Output gate : } \mathbf{o}(t) &= \sigma_S(W_{\text{oh}} \cdot \mathbf{h}(t-1) + W_{\text{ox}} \cdot \mathbf{x}(t) + \mathbf{b}_{\text{o}}) \\
\text{Cell state : } \mathbf{c}(t) &= \mathbf{f}(t) \odot \mathbf{c}(t-1) + \mathbf{i}(t) \odot \mathbf{g}(t) \\
\text{Hidden state : } \mathbf{h}(t) &= \mathbf{o}(t) \odot \tanh(\mathbf{c}(t)) \\
\text{Output : } \mathbf{y}(t) &= W_{\text{hy}} \cdot \mathbf{h}(t) + \mathbf{b}_{\text{y}}
\end{aligned}$$

Here, \odot stands for Hadamard product (element-wise multiplication). Weight matrices W_{ih} , W_{fh} , W_{gh} and W_{oh} have dimensions $\ell \times \ell$. Weight matrices W_{ix} , W_{fx} , W_{gx} and W_{ox} have dimensions $\ell \times m$. Bias terms \mathbf{b}_{i} , \mathbf{b}_{f} , \mathbf{b}_{g} and \mathbf{b}_{o} are $\ell \times 1$ matrices. As before, σ_S and \tanh are the component-wise *activation functions* from \mathbb{R}^{ℓ} to \mathbb{R}^{ℓ} . The input $\mathbf{x}(t)$ is an m -length vector, while $\mathbf{i}(t)$, $\mathbf{f}(t)$, $\mathbf{g}(t)$, $\mathbf{o}(t)$, $\mathbf{c}(t)$ and $\mathbf{h}(t)$ are all ℓ -length vectors.

Similarly, we use \mathbf{i}' , \mathbf{f}' , \mathbf{g}' , \mathbf{o}' , \mathbf{c}' , \mathbf{h}' and \mathbf{y}' to represent parameters of the second LSTM. We also introduce the differences $\delta^{\mathbf{i}}(t)$, $\delta^{\mathbf{f}}(t)$, $\delta^{\mathbf{g}}(t)$, $\delta^{\mathbf{o}}(t)$, $\delta^{\mathbf{c}}(t)$ and $\delta^{\mathbf{h}}(t)$ as vectors of size $\ell \times 1$: For each $\mathbf{v} \in \mathbf{i}, \mathbf{f}, \mathbf{g}, \mathbf{o}, \mathbf{c}, \mathbf{h}$, we have $\delta^{\mathbf{v}}(t) = \mathbf{v}'(t) - \mathbf{v}(t)$.

2.2 Interval Bound Propagation (IBP)

To soundly compute the output values of a neural network for all input values, we represent these values as intervals, and use interval arithmetic to compute their bounds.

³For a scalar input u , $\sigma_S(u) = \frac{e^u}{1+e^u}$, and $\tanh(u) = \frac{e^u - e^{-u}}{e^u + e^{-u}}$.

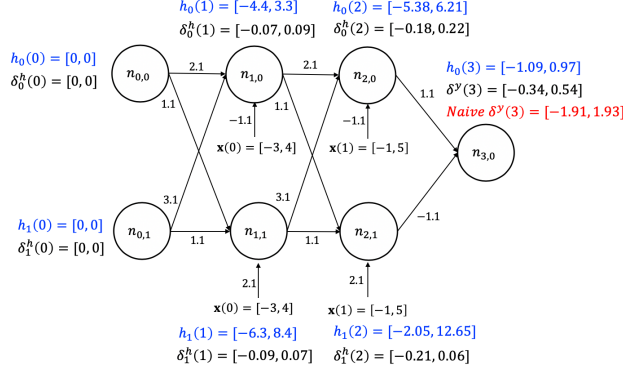


Figure 4: Interval analysis of a recurrent neural network with Sigmoid activation function.

2.2.1 Linear Operations

Given two intervals, e.g., $p \in [a, b]$ and $q \in [c, d]$, the resulting intervals of linear operations such as addition ($p + q$), subtraction ($p - q$), and scaling ($p \cdot c$, where c is a constant) are well defined. That is,

$$\begin{aligned} [a, b] + [c, d] &= [a + c, b + d] \\ [a, b] - [c, d] &= [a - d, b - c] \\ [a, b] \cdot c &= \begin{cases} [a \cdot c, b \cdot c], & c \geq 0 \\ [b \cdot c, a \cdot c], & c < 0 \end{cases} \end{aligned}$$

While the results are sound over-approximations, they may be overly conservative. For example, when $p = 5x$, $q = 4x$ and $x \in [-1, 1]$, since $p - q = 5x - 4x = x$, we know that $(p - q) \in [-1, 1]$, but interval subtraction returns $(p - q) = [-5, 5] - [-4, 4] = [-5 - 4, 5 - (-4)] = [-9, 9]$.

A technique for improving accuracy is the use of symbolic inputs. For example, instead of using the concrete intervals $p \in [-5, 5]$ and $q \in [-4, 4]$, we may use the symbolic upper and lower bounds $p \in [5x, 5x]$ and $q \in [4x, 4x]$, leading to $(p - q) = [5x - 4x, 5x - 4x] = [x, x]$. As a result, we have $(p - q) = [-1, 1]$ after concertizing the symbolic bounds.

In this work, we represent the *symbolic* lower and upper bounds of p as $L(p)$ and $U(p)$, and the concrete lower and upper bounds as \underline{p} and \bar{p} , respectively.

2.2.2 Non-linear Operations

Sound intervals may also be defined for outputs of *Sigmoid* (σ_S) and *Tanh* (\tanh) activation functions. Since both functions are *monotonically increasing*, given a concrete input interval $p = [a, b]$, we have $\sigma(p) \in [\sigma(a), \sigma(b)]$. However, for a symbolic input interval, soundly approximating the output is challenging. In an existing verification tool named CROWN [24], e.g., this is solved by computing linear bounds on the output of each activation function. For LSTMs, the problem is even more challenging because it involves the *product* of nonlinear operations, such as $z = \sigma_S(x) \cdot \tanh(y)$ and $z = x \cdot \sigma_S(y)$. In POPQORN [22], for example, the output is bounded by searching for linear bounding planes of the form $\alpha x + \beta y + \gamma$, where α , β and γ are computed using gradient descent.

In this work, we build upon techniques from CROWN and POPQORN for bounding the output *values* of network f 's neurons, to solve the new problem of *bounding the differences* between two networks f and f' .

3 Overview

In this section, we use an example to illustrate the high-level idea of our method and the shortcomings of state-of-the-art single-network verification techniques for differential verification.

Fig. 4 shows a *many-to-1* Vanilla RNN, f , where all neurons use the *Sigmoid* activation. The entire RNN has 1 hidden layer of 2 neurons, receives a sequence of 2 inputs, and returns a single output. For ease of presentation, the unrolled version of this RNN is shown in Fig. 4 for an input sequence of length 2. Thus, $n_{t,i}$ denotes the i^{th} node in the t^{th} sequence (time step). The initial values in $\mathbf{h}(0)$ and $\delta^{\mathbf{h}}(0)$ are set to 0. The goal is to bound $\delta^{\mathbf{y}}(3)$, the difference between outputs of the original RNN f and a modified RNN f' ; here, $\delta^{\mathbf{y}}(3) = |f'(\mathbf{x}(0), \mathbf{x}(1)) - f(\mathbf{x}(0), \mathbf{x}(1))|$. In

Algorithm 1: Differential Verification of Vanilla RNNs.

Input: network f , network f' , input region X
Output: $\delta^y(T)$

```

1 Init: Initialize  $[L(\mathbf{h}(0)), U(\mathbf{h}(0))]$  and  $[\underline{\delta}^h(0), \overline{\delta}^h(0)]$  to 0
2 for  $t : 1$  to  $T$  do
    // affine transformer
3     Compute  $[L(\mathbf{a}(t)), U(\mathbf{a}(t))]$  and  $[\underline{\delta}^a(t), \overline{\delta}^a(t)]$ ;
    // nonlinear transformer (Algo. 2)
4     Compute  $[L(\mathbf{h}(t)), U(\mathbf{h}(t))]$  and  $[\underline{\delta}^h(t), \overline{\delta}^h(t)]$ ;
5 Compute  $[\underline{\delta}^y(T), \overline{\delta}^y(T)]$ ;

```

this example, the second RNN, f' , is derived from the original RNN f by rounding its edge weights to the nearest whole numbers.

The naïve approach is to leverage an existing verification tool such as POPQORN [22], originally designed to quantify the robustness of a single RNN. As shown for the network in Fig. 2, we can use POPQORN to bound the output of the combined network. For our running example, the bounds computed by POPQORN are $\delta^y(3) = [-1.91, 1.93]$. However, as our analysis shows in this paper, the bounds are overly conservative. The reason is because, to soundly compute the difference $\delta^y(3) = [f'_{low}, f'_{up}] - [f_{low}, f_{up}] = [f'_{low} - f_{up}, f'_{up} - f_{low}]$, POPQORN has to introduce significant approximation error.

DIFFRNN, in contrast, overcomes this problem by pairing neurons and edges of the first network with their counterparts of the second network, and directly computing the difference intervals layer by layer. By directly computing the differences as opposed to the output bounds of the corresponding neurons, we hope to obtain much tighter bounds. However, there are unique challenges in directly bounding the differences. While bounding the non-linear activation function $y = \sigma(x)$ for a single neuron is relatively easy [24], doing so for a pair of neurons at the same time is more difficult because we must bound $z = \sigma(x') - \sigma(x)$, which involves two variables. While we could bound the individual terms $\sigma(x')$ and $\sigma(x)$, and then subtract their bounds, doing so introduces too much approximation error.

To solve the problem, we propose the following new technique. First, we rewrite the difference as $z = \sigma(x + \delta_x) - \sigma(x)$, where x is the value of neuron's output in network f and $\delta_x = (x' - x)$ is the difference between the outputs of two corresponding neurons in f and f' . Given the intervals of x and δ_x , we then examine all possible combinations of their upper and lower bounds, and match these combinations with a set of pre-defined patterns, to soundly compute the interval of z .

For LSTMs, directly bounding the difference $z = x' \cdot \sigma_S(x') - x \cdot \sigma_S(x)$ or $z = \tanh(x') \cdot \sigma_S(x') - \tanh(x) \cdot \sigma_S(x)$ is even more challenging. To the best of our knowledge, no existing verification tool for neural networks can compute tight linear bounds for such functions. Our solution is to formulate them as constrained optimization problems and solve these problems using global optimization tools [25]. In addition, we prove the soundness of these bounds using *dReal*, an off-the-shelf *delta-sat* SMT solver that supports nonlinear constraints.

For the running example, our method would be able to compute the bounds $\delta^y(3) = [-0.34, 0.54]$, which is more than 3X tighter than the bounds computed by POPQORN. The complete results of our experimental comparison with POPQORN will be presented in Section ??.

4 Directly Computing the Difference Interval

Our method for verifying Vanilla RNNs is shown in Algorithm 1. It takes two networks f and f' , the input region X , and a small ϵ as input. After initializing the hidden state and the difference interval, it computes $\mathbf{h}(t)$ and $\delta^h(t)$ of the subsequent layers by applying the affine transformation (i.e., multiplying by the edge weights) followed by performing the non-linear transformation, whose details will be presented in Algo. 2. This is repeated layer by layer, until the output layer is reached. In the end, it computes the final difference interval from $\delta^h(T)$ and $\mathbf{h}(T)$. As mentioned earlier, we leverage the existing tool POPQORN [22] to compute the intervals $\mathbf{h}(t)$, while focusing on computing tight bounds on the differences $\delta^a(t)$ and $\delta^h(t)$.

4.1 Affine Transformer

For Vanilla RNNs, the affine transformation computes each $\delta^a(t)$ in two parts. The first part is caused by the differences between the edge weights in W_{hx} , denoted W_{hx}^Δ , for edges connecting the current input to neurons:

$$\begin{aligned}\delta_t(W_{\text{hx}}) &= W'_{\text{hx}} \cdot \mathbf{x}(t) - W_{\text{hx}} \cdot \mathbf{x}(t) \\ &= W_{\text{hx}}^\Delta \cdot \mathbf{x}(t)\end{aligned}$$

The second part is caused by the differences between the edge weights in W_{hh} , denoted W_{hh}^Δ , for edges connecting the previous hidden states to current hidden states, as well as the differences included in the previous hidden states, denoted $\delta^{\text{h}}(t-1)$.

$$\delta_t(W_{\text{hh}}) = W'_{\text{hh}} \cdot \mathbf{h}'(t-1) - W_{\text{hh}} \cdot \mathbf{h}(t-1)$$

Adding $W'_{\text{hh}} \cdot \mathbf{h}(t-1)$ to the first term and subtracting it from the second term, we get:

$$\begin{aligned}\delta_t(W_{\text{hh}}) &= W'_{\text{hh}} \cdot \mathbf{h}'(t-1) - W_{\text{hh}} \cdot \mathbf{h}(t-1) \\ &\quad + (W'_{\text{hh}} \cdot \mathbf{h}(t-1) - W'_{\text{hh}} \cdot \mathbf{h}(t-1)) \\ &= (W'_{\text{hh}} \cdot \mathbf{h}'(t-1) - W'_{\text{hh}} \cdot \mathbf{h}(t-1)) \\ &\quad + (W'_{\text{hh}} \cdot \mathbf{h}(t-1) - W_{\text{hh}} \cdot \mathbf{h}(t-1)) \\ &= W'_{\text{hh}} \cdot \delta^{\text{h}}(t-1) + W_{\text{hh}}^\Delta \cdot \mathbf{h}(t-1)\end{aligned}$$

$\delta^{\text{a}}(t)$ is then the sum of these two parts:

$$\delta^{\text{a}}(t) = \delta_t(W_{\text{hx}}) + \delta_t(W_{\text{hh}})$$

For LSTMs, the high-level verification procedure is similar to Algo. 1 and is formalized in Algo. 3 in Appendix. The differences for gate $v \in \{\mathbf{i}, \mathbf{f}, \mathbf{g}, \mathbf{o}\}$ within each LSTM cell is computed as follows: $\delta^v(t) = \delta_t(W_{v\text{x}}) + \delta_t(W_{v\text{h}})$.

4.2 Nonlinear Transformer

Vanilla RNN. Here, we define the activation function transformations to compute $\delta^{\text{h}}(t)$ from $\delta^{\text{a}}(t)$. We do so by rewriting the following equation, using the definition of $\delta^{\text{h}}(t)$:

$$\begin{aligned}\delta^{\text{h}}(t) &= \mathbf{h}'(t) - \mathbf{h}(t) \\ &= \sigma(\mathbf{a}'(t)) - \sigma(\mathbf{a}(t)) \\ &= \sigma(\mathbf{a}(t) + \delta^{\text{a}}(t)) - \sigma(\mathbf{a}(t))\end{aligned}$$

where σ is the nonlinear activation function. While RELUDIFF [18] solves this problem for $\sigma = \text{ReLU}$, by exploiting the piece-wise linearity of ReLU , we propose new techniques for $\sigma = \text{Sigmoid}$ or Tanh , as well as composite nonlinear operations built upon them. Note that the technique can be used for other types of monotonic functions as well.

To obtain the tightest linear bounds on $\delta^{\text{h}}(t)$, we formulate this problem as two optimization problems:

$$\begin{aligned}\underline{\delta}^{\text{h}}(t) &= \underset{\mathbf{a}(t), \delta^{\text{a}}(t)}{\text{minimize}} && \sigma_S(\mathbf{a}(t) + \delta^{\text{a}}(t)) - \sigma_S(\mathbf{a}(t)) \\ &\text{subject to} && \mathbf{a}(t) \in [\underline{\mathbf{a}}(t), \bar{\mathbf{a}}(t)], \delta^{\text{a}}(t) \in [\underline{\delta}^{\text{a}}(t), \bar{\delta}^{\text{a}}(t)]\end{aligned}$$

$$\begin{aligned}\bar{\delta}^{\text{h}}(t) &= \underset{\mathbf{a}(t), \delta^{\text{a}}(t)}{\text{maximize}} && \sigma_S(\mathbf{a}(t) + \delta^{\text{a}}(t)) - \sigma_S(\mathbf{a}(t)) \\ &\text{subject to} && \mathbf{a}(t) \in [\underline{\mathbf{a}}(t), \bar{\mathbf{a}}(t)], \delta^{\text{a}}(t) \in [\underline{\delta}^{\text{a}}(t), \bar{\delta}^{\text{a}}(t)]\end{aligned}$$

These are two-variable optimization problems of the form $f(x, d) = \sigma_S(x + d) - \sigma_S(x)$, which are expensive to solve at run time. To reduce the computational cost, we propose to reduce them first to single-variable optimization problems, by leveraging the fact that $f(x, d)$ is monotonic with respect to d . Our goal is to compute the maximum and minimum of $f(x, d) = \sigma_S(x + d) - \sigma_S(x)$, where $x \in [x_l, x_u]$ and $d \in [d_l, d_u]$. Due to the monotonicity of $f(x, d)$ with respect to d , we know that the minimum always occurs when $d = d_l$ and the maximum occurs when $d = d_u$. Thus, the problem is reduced to finding the maximum and minimum of $f(x, d)$ for a fixed $d = d_l$ or $d = d_u$.

Depending on the actual value of d being either positive or negative, the function $f(x, d)$ will be one of the two forms illustrated in Fig. 5.

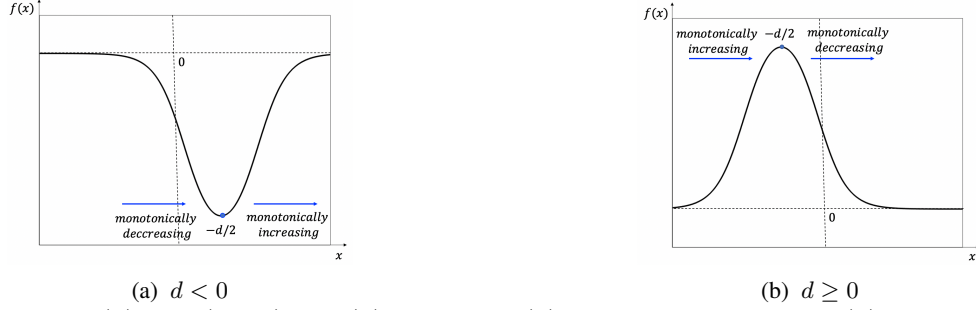


Figure 5: $f(x) = \sigma_S(x + d) - \sigma_S(x)$. (a) shows $f(x)$ for $d < 0$ and (b) shows $f(x)$ for $d \geq 0$.

Thus, to compute the minimum of $f(x, d)$, there are three cases to consider when d_l is positive, and another three cases to consider when d_l is negative. For instance, when $d_l \leq 0$ (Fig. 5a), if $x_l \leq x_u \leq -d_l/2$, since $f(x, d_l)$ is monotonically decreasing in this region, we have $\min(f(x, d_l)) = f(x_u, d_l)$; if $x_l \leq -d_l/2 \leq x_u$, we have $\min(f(x, d_l)) = f(-d_l/2, d_l)$; and if $-d_l/2 \leq x_l \leq x_u$ (monotonically increasing), we have $\min(f(x, d_l)) = f(x_l, d_l)$. The main advantage is that, by plugging in the bounds of x and d , we get the bounds of $f(x, d)$ immediately, without the need to solve any optimization problem at run time.

To compute $\delta^h(t)$ and $\bar{\delta}^h(t)$, there are 12 cases in total, the details of which are formalized in Algo. 2. For *Tanh* (tanh), the 12 cases are exactly the same as those for *Sigmoid* (σ_S); thus, we omit them for brevity⁴.

The final difference interval for Vanilla RNNs is computed from $\delta^h(T)$ and $\mathbf{h}(T)$ as follows:

$$\delta^y = W'_{hy} \cdot \delta^h(T) + W_{hy}^\Delta \cdot \mathbf{h}(T)$$

LSTM. Next, we consider computing $\delta^h(t)$ for LSTMs. First, we need to compute $\delta^c(t)$. In the following computations, we add underscore “in” to denote the value of each variable after the affine transform but before the nonlinear activation. Based on the definition of $\delta^c(t)$, we have

$$\delta^c(t) = \mathbf{c}'(t) - \mathbf{c}(t) \quad (4)$$

,where $\mathbf{c}'(t)$ and $\mathbf{c}(t)$ are intervals of the cell states for t^{th} sequence. Based on the definition of the cell state, we have

$$\begin{aligned} \mathbf{c}'(t) &= \sigma_S(\mathbf{f}'_{in}(t)) \odot \mathbf{c}'(t-1) + \sigma_S(\mathbf{i}'_{in}(t)) \odot \tanh(\mathbf{g}'_{in}(t)) \\ \mathbf{c}(t) &= \sigma_S(\mathbf{f}_{in}(t)) \odot \mathbf{c}(t-1) + \sigma_S(\mathbf{i}_{in}(t)) \odot \tanh(\mathbf{g}_{in}(t)) \end{aligned}$$

After replacing the above equation for $\mathbf{c}'(t)$ and $\mathbf{c}(t)$ in (4) and simplification, we have

$$\begin{aligned} \delta^c(t) &= \sigma_S(\mathbf{f}'_{in}(t)) \odot \mathbf{c}'(t-1) - \sigma_S(\mathbf{f}_{in}(t)) \odot \mathbf{c}(t-1) \\ &\quad + \sigma_S(\mathbf{i}'_{in}(t)) \odot \tanh(\mathbf{g}'_{in}(t)) - \sigma_S(\mathbf{i}_{in}(t)) \odot \tanh(\mathbf{g}_{in}(t)), \end{aligned}$$

⁴For non-monotonic activation functions we can compute the maximum and minimum using off-the-shelf global optimization tools and then validate the computed bounds using SMT solvers.

Algorithm 2: Over-approximating Non-linear Activation.

Input: value $[L(\mathbf{a}(t)), U(\mathbf{a}(t))]$, difference $[\underline{\delta}^{\mathbf{a}}(t), \overline{\delta}^{\mathbf{a}}(t)]$
Output: value $[L(\mathbf{h}(t)), U(\mathbf{h}(t))]$, difference $[\underline{\delta}^{\mathbf{h}}(t), \overline{\delta}^{\mathbf{h}}(t)]$

```

// Computing  $\mathbf{h}(t)$ 
// Using a previous work POPQORN
1  $[L(\mathbf{h}(t)), U(\mathbf{h}(t))] = \text{POPQORN.NonLinearTransformer}([L(\mathbf{a}(t)), U(\mathbf{a}(t))]);$  // Computing  $\underline{\delta}^{\mathbf{h}}(t)$ 
2 if  $\underline{\delta}^{\mathbf{a}}(t) \geq 0$  then
    if  $\overline{\mathbf{a}}(t) \leq -\underline{\delta}^{\mathbf{a}}(t)/2$  then
         $\underline{\delta}^{\mathbf{h}}(t) = \sigma_S(\underline{\mathbf{a}}(t) + \underline{\delta}^{\mathbf{a}}(t)) - \sigma_S(\underline{\mathbf{a}}(t));$ 
    else if  $\underline{\mathbf{a}}(t) \geq -\underline{\delta}^{\mathbf{a}}(t)/2$  then
3          $\underline{\delta}^{\mathbf{h}}(t) = \sigma_S(\overline{\mathbf{a}}(t) + \underline{\delta}^{\mathbf{a}}(t)) - \sigma_S(\overline{\mathbf{a}}(t));$ 
    else
         $a = \sigma_S(\overline{\mathbf{a}}(t) + \underline{\delta}^{\mathbf{a}}(t)) - \sigma_S(\overline{\mathbf{a}}(t));$ 
         $b = \sigma_S(\underline{\mathbf{a}}(t) + \underline{\delta}^{\mathbf{a}}(t)) - \sigma_S(\underline{\mathbf{a}}(t));$ 
         $\underline{\delta}^{\mathbf{h}}(t) = \min(a, b);$ 
4 else
    if  $\overline{\mathbf{a}}(t) \leq -\underline{\delta}^{\mathbf{a}}(t)/2$  then
         $\underline{\delta}^{\mathbf{h}}(t) = \sigma_S(\overline{\mathbf{a}}(t) + \underline{\delta}^{\mathbf{a}}(t)) - \sigma_S(\overline{\mathbf{a}}(t));$ 
5     else if  $\underline{\mathbf{a}}(t) \geq -\underline{\delta}^{\mathbf{a}}(t)/2$  then
         $\underline{\delta}^{\mathbf{h}}(t) = \sigma_S(\underline{\mathbf{a}}(t) + \underline{\delta}^{\mathbf{a}}(t)) - \sigma_S(\underline{\mathbf{a}}(t));$ 
    else
         $\underline{\delta}^{\mathbf{h}}(t) = \sigma_S(-\underline{\delta}^{\mathbf{a}}(t)/2 + \underline{\delta}^{\mathbf{a}}(t)) - \sigma_S(-\underline{\delta}^{\mathbf{a}}(t)/2);$ 
// Computing  $\overline{\delta}^{\mathbf{h}}(t)$ 
6 if  $\overline{\delta}^{\mathbf{a}}(t) \geq 0$  then
    if  $\overline{\mathbf{a}}(t) \leq -\overline{\delta}^{\mathbf{a}}(t)/2$  then
         $\overline{\delta}^{\mathbf{h}}(t) = \sigma_S(\overline{\mathbf{a}}(t) + \overline{\delta}^{\mathbf{a}}(t)) - \sigma_S(\overline{\mathbf{a}}(t));$ 
7     else if  $\underline{\mathbf{a}}(t) \geq -\overline{\delta}^{\mathbf{a}}(t)/2$  then
         $\overline{\delta}^{\mathbf{h}}(t) = \sigma_S(\underline{\mathbf{a}}(t) + \overline{\delta}^{\mathbf{a}}(t)) - \sigma_S(\underline{\mathbf{a}}(t));$ 
    else
         $\overline{\delta}^{\mathbf{h}}(t) = \sigma_S(-\overline{\delta}^{\mathbf{a}}(t)/2 + \overline{\delta}^{\mathbf{a}}(t)) - \sigma_S(-\overline{\delta}^{\mathbf{a}}(t)/2);$ 
8 else
    if  $\overline{\mathbf{a}}(t) \leq -\overline{\delta}^{\mathbf{a}}(t)/2$  then
         $\overline{\delta}^{\mathbf{h}}(t) = \sigma_S(\underline{\mathbf{a}}(t) + \overline{\delta}^{\mathbf{a}}(t)) - \sigma_S(\underline{\mathbf{a}}(t));$ 
    else if  $\underline{\mathbf{a}}(t) \geq -\overline{\delta}^{\mathbf{a}}(t)/2$  then
9          $\overline{\delta}^{\mathbf{h}}(t) = \sigma_S(\overline{\mathbf{a}}(t) + \overline{\delta}^{\mathbf{a}}(t)) - \sigma_S(\overline{\mathbf{a}}(t));$ 
    else
         $a = \sigma_S(\overline{\mathbf{a}}(t) + \overline{\delta}^{\mathbf{a}}(t)) - \sigma_S(\overline{\mathbf{a}}(t));$ 
         $b = \sigma_S(\underline{\mathbf{a}}(t) + \overline{\delta}^{\mathbf{a}}(t)) - \sigma_S(\underline{\mathbf{a}}(t));$ 
         $\overline{\delta}^{\mathbf{h}}(t) = \max(a, b);$ 

```

where each variable is an interval. Since the above equation contains eight variables, manually enumerating all possible solutions at the design time is practically infeasible. Thus, we have to compute them at run time. To make the problem tractable, we divide $\delta^{\mathbf{c}}(t)$ into two parts, each with four variables, and optimize them independently. We define the two parts as follows:

$$\begin{aligned}\delta_1^{\mathbf{c}}(t) &= \sigma_S(\mathbf{f}'_{in}(t)) \odot \mathbf{c}'(t-1) - \sigma_S(\mathbf{f}_{in}(t)) \odot \mathbf{c}(t-1) \\ \delta_2^{\mathbf{c}}(t) &= \sigma_S(\mathbf{i}'_{in}(t)) \odot \tanh(\mathbf{g}'_{in}(t)) - \sigma_S(\mathbf{i}_{in}(t)) \odot \tanh(\mathbf{g}_{in}(t))\end{aligned}$$

Since $\mathbf{f}'_{in}(t) = \mathbf{f}_{in}(t) + \delta^{\mathbf{f}}_{in}(t)$, $\mathbf{i}'_{in}(t) = \mathbf{i}_{in}(t) + \delta^{\mathbf{i}}_{in}(t)$, $\mathbf{g}'_{in}(t) = \mathbf{g}_{in}(t) + \delta^{\mathbf{g}}_{in}(t)$ and $\mathbf{c}'(t-1) = \mathbf{c}(t-1) + \delta^{\mathbf{c}}_{in}(t-1)$, we can rewrite $\delta_1^{\mathbf{c}}(t)$ and $\delta_2^{\mathbf{c}}(t)$ as follows:

$$\begin{aligned}
\delta_1^c(t) &= \sigma_S(\mathbf{f}_{in}(t) + \delta_{in}^f(t)) \odot (\mathbf{c}(t-1) + \delta_{in}^c(t-1)) \\
&\quad - \sigma_S(\mathbf{f}_{in}(t)) \odot \mathbf{c}(t-1) \\
\delta_2^c(t) &= \sigma_S(\mathbf{i}_{in}(t) + \delta_{in}^i(t)) \odot \tanh(\mathbf{g}_{in}(t) + \delta_{in}^g(t)) \\
&\quad - \sigma_S(\mathbf{i}_{in}(t)) \odot \tanh(\mathbf{g}_{in}(t)) \\
\overline{\delta}^c(t) &= \overline{\delta}_1^c(t) + \overline{\delta}_2^c(t) \\
\underline{\delta}^c(t) &= \underline{\delta}_1^c(t) + \underline{\delta}_2^c(t)
\end{aligned}$$

To reduce notational complexity, we rewrite the above equations as $f_1(x, d_x, y, d_y) = \sigma_S(x + d_x) \cdot (y + d_y) - \sigma_S(x) \cdot y$ and $f_2(x, d_x, y, d_y) = \sigma_S(x + d_x) \cdot \tanh(y + d_y) - \sigma_S(x) \cdot \tanh(y)$. Observing that both equations are monotonic with respect to d_y , we convert the four-variable optimization problems to three variables. We first rewrite f_1 as:

$$\begin{aligned}
f_1(x, d_x, y, d_y) &= \sigma_S(x + d_x) \cdot y + \sigma_S(x + d_x) \cdot d_y - \sigma_S(x) \cdot y \\
&= (\sigma_S(x + d_x) - \sigma_S(x)) \cdot y + \sigma_S(x + d_x) \cdot d_y
\end{aligned}$$

Now, since $\sigma_S(x + d_x) \geq 0$, the maximum of f_1 occurs when $d_y = \overline{d}_y$ and the minimum of f_1 happens at $d_y = \underline{d}_y$, we can treat d_y as a constant. Similarly, for f_2 , since $\sigma_S(x + d_x) \geq 0$ and $\tanh(y + d_y)$ is monotonically increasing, the maximum and minimum of f_2 happens when $d = \overline{d}_y$ and $d = \underline{d}_y$, respectively. Finally, to obtain $\delta^h(t)$, we solve two 4-variable optimization problems:

$$\begin{aligned}
\delta^h(t) &= \sigma_S(\mathbf{o}_{in}(t) + \delta_{in}^o(t)) \odot \tanh(\mathbf{c}(t) + \delta^c(t)) \\
&\quad - \sigma_S(\mathbf{o}_{in}(t)) \odot \tanh(\mathbf{c}(t)) \\
\overline{\delta}^h(t) &= \max(\delta^h(t)) \\
\underline{\delta}^h(t) &= \min(\delta^h(t))
\end{aligned}$$

These functions are again of the form $f_2(x, d_x, y, d_y) = \sigma_S(x + d_x) \cdot \tanh(y + d_y) - \sigma_S(x) \cdot \tanh(y)$ and thus can be converted to 3-variable optimization problems. We use off-the-shelf global optimization tools, which are written in Python and based on differential evolution (DE) [25], to solve these optimization problems. In evolutionary computation, DE is a method that optimizes a problem by iteratively trying to improve a candidate solution with regard to a given measure of quality. After that, we use *dReal* [19], which is a *delta-sat* SMT solver with support for nonlinear functions, to validate the computed bounds. If the bounds are not yet sound according to *dReal*, we slightly increase the maximum or decrease the minimum until they are proved to be sound (see Algo. 4 in Appendix). The final difference interval for LSTMs is derived in a way that is similar to Vanilla RNNs. The details are formalized in Algo. 3 and Algo. 4 in Appendix.

5 Experiments

Benchmarks. Our benchmarks are 12 feed forward neural networks with *Sigmoid* and *Tanh* activations⁵, 12 Vanilla RNNs, and 6 LSTMs trained using the MNIST [20] and Human Activity Recognition (HAR) [21] data sets. From each network f , we produce f' by rounding the edge weights of f from 32-bit floats to 16-bit floats. We generate the input regions for differential verification using global perturbation [26] or targeted pixel perturbation [27]. We randomly take 100 test inputs, and for each one, we allow each of the inputs to be perturbed $-/+1\%$ of the whole range (*global* perturbation), or we randomly pick 3 *inputs* and set their range to the whole range (*targeted* perturbation). Given an input region, the goal is to verify the difference of at most ϵ between the outputs of f and f' . The value of ϵ is specified for each benchmark separately.

MNIST. MNIST is one of the most popular data sets for handwritten digits recognition, consisting of 60,000 and 10,000 images corresponding to training and test data. The images are $28 \times 28 = 784$ pixels, and each pixel has a grayscale value

⁵One of our evaluation objectives is to extend the results of RELUDIFF to general activation functions instead of *ReLU*s. This also allows us to validate our methodology in the relatively simpler world of feedforward networks before tackling RNNs.

in the range $[0, 255]$ which is usually scaled to $[-1, 1]$. The neural networks trained on this data set generate 10 outputs typically in the range $[-10, 10]$ and the digit with the highest score is the chosen classification.

Human Activity recognition. HAR is a labeled time-series data set used to train models for human activity recognition. The data is recorded from accelerometer and gyroscope sensors in waist-mounted smartphones. In total, 561 input statistics are computed from these two sensors including max, min, mean, etc., which are normalized to the range $[-1, 1]$. This data is obtained from the recordings of 30 subjects performing six activities: walking, walking upstairs, walking downstairs, sitting, standing, and laying down. The network trained on this data set takes 561 inputs and generates 6 outputs typically in the range $[-20, 20]$. The output with the maximum value is the predicted class.

Experimental Evaluation. We run the experiments on an Intel Core-i7 Macbook Pro with 2.7 GHz processors and 16 GB RAM. Timeout for each verification problem is set to 30 minutes. We compare the results of feed-forward networks with CROWN [24] which is the state-of-the-art verification tool for a single feed-forward neural network.

Among the existing tools for verifying a single RNN [28, 29], we find empirically that POPQORN is significantly more accurate than those from [28, 29]: the bounds computed by [28, 29] often have too much approximation error, and hence would give too many false positives for the differential verification problem. Therefore, we compare our experimental results on RNNs with POPQORN, which leverages gradient descent techniques to compute linear bounds on nonlinear surfaces $x \cdot \sigma_S(y)$ and $\sigma_S(x) \cdot \tanh(y)$. As POPQORN evaluates bounds using numerical tools based on gradient descent, while the approach is sound in theory, it is susceptible to numerical precision issues. Hence, we added an extra validation step using *dReal* to ensure numerical precision of the bounds computed by POPQORN.

Results. In the 3000 differential verification problems that we consider, DIFFRNN can verify 2887 out of 3000 problems and is faster than CROWN and POPQORN in more than 93% of the cases. CROWN and POPQORN in total can verify only 1140 out of 3000 problems. DIFFRNN returns *Unknown* for other 123 verification problems that cannot verify.

Table. 1 shows the results of differential verification of feed-forward neural networks with *Sigmoid* activation trained on MNIST data set. The networks have 3 structures 3×128 (3 hidden layers of 128 neurons), 2×512 (2 hidden layers of 512 neurons) and 4×1024 (4 hidden layers of 1024 neurons). Thus, the networks have 2, 3 and 4 layers in addition to input and output layers. The goal is to verify the difference of at most 1 ($\epsilon = 1$) between the outputs of f and f' . Among the 600 verification problems shown in Table. 1, DIFFRNN verified all of them while CROWN verified only 224.

Table. 2 shows the results of differential verification of feed-forward neural networks with *Tanh* activation and three types of structures: 3×128 , 2×1024 and 4×512 on the HAR data set. DIFFRNN verified 591 of the 600 cases for $\epsilon = 2$ as apposed to the 282 cases verified by CROWN.

Table. 3 shows the results of verifying Vanilla RNNs with $\epsilon = 1$ on the MNIST data set. The network structures are 4×128 (4 sequences of 128 neurons), 7×32 (7 sequences of 32 neurons) and 14×8 (14 sequences of 8 neurons). Among the 600 verification problems, DIFFRNN verified 502 while POPQORN only verified 156.

Table. 4 shows the results of verifying Vanilla RNNs on the HAR data set. The networks are 3×32 , 3×128 and 11×8 and $\epsilon = 2$. DIFFRNN was faster than POPQORN in all cases and also verified more properties (598/600), while POPQORN only verified 478 properties.

Finally, Table. 5 shows the results of verifying LSTMs trained on the HAR data set for structures 3×32 , 3×64 and 11×8 and $\epsilon = 0.1$. The results again show that DIFFRNN was better: it verified all 600 cases while POPQORN can verify none of them.

Benchmark	DIFFRNN (New)	CROWN	Avg. Speedup
dnn-3x128-global	100/100, 22.7s	1/100, 25.9s	1.14
dnn-2x512-global	100/100, 52.4s	7/100, 61.9s	1.18
dnn-4x1024-global	100/100, 207.8s	0/100, 246.9s	1.27
dnn-3x128-3-inputs	100/100, 16.5s	79/100, 18.9	1.14
dnn-2x512-3-inputs	100/100, 44.5s	100/100, 49.8s	1.11
dnn-4x1024-3-inputs	100/100, 197.6s	37/100, 204.9s	1.03

Table 1: Verified problems, totall verification problems and Avg verification time (seconds) (\cdot/\cdot), \cdot of DIFFRNN and CROWN on MNIST for DNN with Sigmoid activation and $\epsilon = 1$.

We also applied differential verification to 3 LSTM structures 4×128 , 7×32 and 14×8 on the MNIST data set. Neither DIFFRNN nor POPQORN could verify any of these problems. The reason behind the failure of DIFFRNN is that, after 2 sequences of propagation, the difference intervals start to get loose, resulting in poor performance of

Benchmark	DIFFRNN(New)	CROWN	Avg. Speedup
dnn-3x128-global	100/100, 18.4s	51/100, 22.2s	1.20
dnn-2x1024-global	100/100, 118.5s	33/100, 147.4s	1.24
dnn-4x512-global	91/100, 160.2s	0/100, 218.2s	1.36
dnn-3x128-3-inputs	100/100, 16.0s	98/100, 19.0s	1.19
dnn-2x1024-3-inputs	100/100, 96.1s	100/100, 122.1s	1.27
dnn-4x512-3-inputs	100/100, 123.2s	0/100, 162.3s	1.31

Table 2: Verified problems, total verification problems and Avg verification time (seconds) (\cdot/\cdot), \cdot of DIFFRNN and CROWN on HAR for DNN with Tanh activation and $\epsilon = 2$.

Benchmark	DIFFRNN (New)	POPQORN	Avg. Speedup
rnn-4x128-global	100/100, 562.9s	0/100, 1148.7s	2.04
rnn-7x32-global	57/100, 75.1s	0/100, 136.1s	1.81
rnn-14x8-global	50/100, 14.1s	15/100, 24.4s	1.72
rnn-4x128-3-inputs	100/100, 571.8s	54/100, 1121.9s	1.96
rnn-7x32-3-inputs	100/100, 74.2s	15/100, 128.3s	1.72
rnn-14x8-3-inputs	95/100, 16.2s	57/100, 24.3s	1.49

Table 3: Verified problems, total verification problems and Avg verification time (seconds) (\cdot/\cdot), \cdot of DIFFRNN and POPQORN on MNIST for Vanilla RNN with Tanh activation and $\epsilon = 1$.

the *dReal* SMT solver. As *dReal* is an interval constraint based solver, bigger intervals requires *dReal* to reason over bigger regions of space. While POPQORN was actually faster than DIFFRNN in this experiment, the final differences it computed are too loose and cannot verify the equivalence of any two networks for $\epsilon \leq 20$. Thus, the results point to directions for future research.

While in general DIFFRNN achieves a significant performance gain compared to the state-of-the-art verification tools for a single RNN, such as POPQORN, it can only tightly bound similarity of two 1-layer RNNs with up to 20 input sequences. To the best of our knowledge, there is no existing technique based on IBP that can certify multi-layer RNNs with long input sequences. POPQORN, [28] and [29] that are tools for quantifying the robustness of a single RNN can only certify the robustness for 1-layer RNNs. The reason is because IBP starts to get loose as the number of sequences or layers increases. In DIFFRNN, we are dealing with two RNNs at the same time, thus, the problem is twice harder. For example, 2-variable optimization problems in POPQORN correspond to 4-variable optimization problems in DIFFRNN.

6 Related work

RELUDIFF [18] is currently the only tool that can verify neural networks in the differential setting. However, unlike our approach, RELUDIFF does not solve the many challenges that are unique to RNNs. More generally, our work falls into the category of techniques for improving safety, security, and reliability in deep learning. Along this line, there has been a significant amount of research that we can classify into two broad categories: (1) techniques for discovering misbehaviors, and (2) techniques for proving the absence of misbehaviors, like DIFFRNN. We review a representative set of these works here.

Techniques along the first line are often geared towards finding *adversarial examples* [5,6]. There have been many works using machine learning techniques such as gradient-based optimization and even generative adversarial networks [4,7–9]. In addition, other techniques use white-box heuristics [12–15, 30, 31] such as neuron coverage or various black-box techniques [16, 17, 32]. While useful for discovering misbehavior they do not guarantee the absence of misbehavior, which we do.

Techniques along the second line usually aim to *prove the absence of* adversarial examples. For example, many works have developed exact and complete techniques that are guaranteed to *eventually* terminate with the correct result. They have used LP solvers [33–38], built specialized solvers for neural networks [27, 39, 40], or combined approximation techniques with refinement [41–43].

Others have focused solely on approximation techniques [3, 24, 26, 44, 45], which often use abstract domains [46], such as intervals [47], zonotopes [48], and polyhedra [49]. Only very recent works have attempted to verify RNNs [22, 28, 29], but, as we have shown, they do not perform well in the differential setting.

Benchmark	DIFFRNN (New)	POPQORN	Avg. Speedup
rnn-3x32-global	100/100, 28.4s	60/100, 58.5s	2.05
rnn-3x128-global	100/100, 424.8s	74/100, 849.0s	1.99
rnn-11x8-global	100/100, 11.6s	62/100, 18.0s	1.54
rnn-3x32-3-inputs	100/100, 29.0s	99/100, 57.8s	1.98
rnn-3x128-3-inputs	100/100, 424.8s	98/100, 825.5s	1.94
rnn-11x8-3-inputs	98/100, 11.6s	85/100, 17.3s	1.48

Table 4: Verified problems, totall verification problems and Avg verification time (seconds) (\cdot/\cdot), \cdot of DIFFRNN and POPQORN on HAR for Vanilla RNN with Tanh activation and $\epsilon = 2$.

Benchmark	DIFFRNN (New)	POPQORN	Avg. Speedup
lstm-3x32-global	100/100, 15512.6s	0/100, 16020.2s	1.03
lstm-3x64-global	100/100, 23602.9s	0/100, 18828.5s	0.79
lstm-11x8-global	100/100, 34766.3s	0/100, 35519.1s	1.02
lstm-3x32-3-inputs	100/100, 11820.0s	0/100, 14716.0s	1.24
lstm-3x64-3-inputs	100/100, 18789.0s	0/100, 17868.7s	0.95
lstm-11x8-3-inputs	100/100, 23224.1s	0/100, 33398.0s	1.43

Table 5: Verified problems, totall verification problems and Avg verification time (seconds) (\cdot/\cdot), \cdot of DIFFRN and POPQORN on HAR for LSTM and $\epsilon = 0.1$.

In addition, these techniques have been integrated into the training process to produce more robust and verifiable networks [50–54]. We believe a similar approach could be taken to produce networks more amenable to differential verification. We leave this as future work.

7 Conclusion

We have presented DIFFRNN, the first method for differential verification of two closely related recurrent neural networks. By reasoning about general nonlinear activation functions, our work goes beyond previous approaches for differential verification such as RELUDIFF (that used only *ReLU* activations). More crucially, we show how we can extend our approach to a more general class of NNs, known as recurrent neural networks. DIFFRNN leverages interval analysis to directly and more accurately compute difference in the values of neurons of the two networks from the input layer to output layer. At each step, the soundness of the computed differences is validated using a nonlinear *delta-sat* SMT solver. Our experimental comparison of DIFFRNN with state-of-the-art verification tools such as CROWN and POPQORN show that the proposed method not only is faster but also can verify significantly more properties.

References

- [1] Mariusz Bojarski, Davide Del Testa, Daniel Dworakowski, Bernhard Firner, Beat Flepp, Praseon Goyal, Lawrence D Jackel, Mathew Monfort, Urs Muller, Jiakai Zhang, et al. End to end learning for self-driving cars. *arXiv preprint arXiv:1604.07316*, 2016.
- [2] Kyle D Julian, Mykel J Kochenderfer, and Michael P Owen. Deep neural network compression for aircraft collision avoidance systems. *Journal of Guidance, Control, and Dynamics*, 42(3):598–608, 2019.
- [3] Zhaoyang Lyu, Ching-Yun Ko, Zhifeng Kong, Ngai Wong, Dahua Lin, and Luca Daniel. Fastened crown: Tightened neural network robustness certificates. *arXiv preprint arXiv:1912.00574*, 2019.
- [4] Ian J. Goodfellow, Jonathon Shlens, and Christian Szegedy. Explaining and harnessing adversarial examples. In *International Conference on Learning Representations*, 2015.
- [5] Christian Szegedy, Wojciech Zaremba, Ilya Sutskever, Joan Bruna, Dumitru Erhan, Ian Goodfellow, and Rob Fergus. Intriguing properties of neural networks. *arXiv preprint arXiv:1312.6199*, 2013.
- [6] Alexey Kurakin, Ian J. Goodfellow, and Samy Bengio. Adversarial examples in the physical world. In *International Conference on Learning Representations*, 2017.
- [7] Seyed-Mohsen Moosavi-Dezfooli, Alhussein Fawzi, and Pascal Frossard. DeepFool: A simple and accurate method to fool deep neural networks. In *IEEE Conference on Computer Vision and Pattern Recognition*, pages 2574–2582, 2016.

- [8] Anh Mai Nguyen, Jason Yosinski, and Jeff Clune. Deep neural networks are easily fooled: High confidence predictions for unrecognizable images. In *IEEE Conference on Computer Vision and Pattern Recognition*, pages 427–436, 2015.
- [9] Weilin Xu, Yanjun Qi, and David Evans. Automatically evading classifiers: A case study on PDF malware classifiers. In *Network and Distributed System Security Symposium*, 2016.
- [10] Song Han, Huizi Mao, and William J. Dally. Deep compression: Compressing deep neural network with pruning, trained quantization and huffman coding. In *International Conference on Learning Representations*, 2016.
- [11] Yu Cheng, Duo Wang, Pan Zhou, and Tao Zhang. A survey of model compression and acceleration for deep neural networks. *arXiv preprint arXiv:1710.09282*, 2017.
- [12] Lei Ma, Felix Juefei-Xu, Fuyuan Zhang, Jiyuan Sun, Minhui Xue, Bo Li, Chunyang Chen, Ting Su, Li Li, Yang Liu, et al. Deepgauge: Multi-granularity testing criteria for deep learning systems. In *IEEE/ACM International Conference On Automated Software Engineering*, pages 120–131. ACM, 2018.
- [13] Kexin Pei, Yinzhi Cao, Junfeng Yang, and Suman Jana. Deepxplore: Automated whitebox testing of deep learning systems. In *ACM symposium on Operating Systems Principles*, pages 1–18, 2017.
- [14] Yuchi Tian, Kexin Pei, Suman Jana, and Baishakhi Ray. Deeptest: Automated testing of deep-neural-network-driven autonomous cars. In *International Conference on Software Engineering*, pages 303–314, 2018.
- [15] Augustus Odena and Ian Goodfellow. Tensorfuzz: Debugging neural networks with coverage-guided fuzzing. *arXiv preprint arXiv:1807.10875*, 2018.
- [16] Xiaofei Xie, Lei Ma, Felix Juefei-Xu, Minhui Xue, Hongxu Chen, Yang Liu, Jianjun Zhao, Bo Li, Jianxiong Yin, and Simon See. Deephunter: a coverage-guided fuzz testing framework for deep neural networks. In *Proceedings of the 28th ACM SIGSOFT International Symposium on Software Testing and Analysis*, pages 146–157, 2019.
- [17] Xiaofei Xie, Lei Ma, Haijun Wang, Yuekang Li, Yang Liu, and Xiaohong Li. Diffchaser: Detecting disagreements for deep neural networks. In *Proceedings of the 28th International Joint Conference on Artificial Intelligence*, pages 5772–5778. AAAI Press, 2019.
- [18] Brandon Paulsen, Jingbo Wang, and Chao Wang. Reludiff: Differential verification of deep neural networks. *arXiv preprint arXiv:2001.03662*, 2020.
- [19] Sicun Gao, Soonho Kong, and Edmund M Clarke. dreal: An smt solver for nonlinear theories over the reals. In *International conference on automated deduction*, pages 208–214. Springer, 2013.
- [20] Yann LeCun and Corinna Cortes. MNIST handwritten digit database. 2010.
- [21] Davide Anguita, Alessandro Ghio, Luca Oneto, Xavier Parra, and Jorge Luis Reyes-Ortiz. A public domain dataset for human activity recognition using smartphones. In *Esann*, 2013.
- [22] Ching-Yun Ko, Zhaoyang Lyu, Tsui-Wei Weng, Luca Daniel, Ngai Wong, and Dahua Lin. Popqorn: Quantifying robustness of recurrent neural networks. *arXiv preprint arXiv:1905.07387*, 2019.
- [23] Tristan Stérin, Nicolas Farrugia, and Vincent Gripon. An intrinsic difference between vanilla rnns and gru models. *COGNITIVE 2017*, page 84, 2017.
- [24] Huan Zhang, Tsui-Wei Weng, Pin-Yu Chen, Cho-Jui Hsieh, and Luca Daniel. Efficient neural network robustness certification with general activation functions. In *Annual Conference on Neural Information Processing Systems*, pages 4939–4948, 2018.
- [25] Kenneth Price, Rainer M Storn, and Jouni A Lampinen. *Differential evolution: a practical approach to global optimization*. Springer Science & Business Media, 2006.
- [26] Gagandeep Singh, Timon Gehr, Markus Püschel, and Martin T. Vechev. An abstract domain for certifying neural networks. *ACM SIGACT-SIGPLAN Symposium on Principles of Programming Languages*, pages 41:1–41:30, 2019.
- [27] Divya Gopinath, Guy Katz, Corina S. Pasareanu, and Clark W. Barrett. DeepSafe: A data-driven approach for assessing robustness of neural networks. In *Automated Technology for Verification and Analysis - 16th International Symposium, ATVA 2018, Los Angeles, CA, USA, October 7-10, 2018, Proceedings*, pages 3–19, 2018.
- [28] Robin Jia, Aditi Raghunathan, Kerem Göksel, and Percy Liang. Certified robustness to adversarial word substitutions. *arXiv preprint arXiv:1909.00986*, 2019.
- [29] Zhouxing Shi, Huan Zhang, Kai-Wei Chang, Minlie Huang, and Cho-Jui Hsieh. Robustness verification for transformers. *arXiv preprint arXiv:2002.06622*, 2020.
- [30] Shiqing Ma, Yingqi Liu, Wen-Chuan Lee, Xiangyu Zhang, and Ananth Grama. MODE: automated neural network model debugging via state differential analysis and input selection. In *Proceedings of the 2018 ACM Joint Meeting on European Software Engineering Conference and Symposium on the Foundations of Software Engineering, ESEC/SIGSOFT FSE 2018, Lake Buena Vista, FL, USA, November 04-09, 2018*, pages 175–186, 2018.
- [31] Youcheng Sun, Min Wu, Wenjie Ruan, Xiaowei Huang, Marta Kwiatkowska, and Daniel Kroening. Concolic testing for deep neural networks. In *Proceedings of the 33rd ACM/IEEE International Conference on Automated Software Engineering, ASE 2018, Montpellier, France, September 3-7, 2018*, pages 109–119, 2018.

- [32] Matthew Wicker, Xiaowei Huang, and Marta Kwiatkowska. Feature-guided black-box safety testing of deep neural networks. In *International Conference on Tools and Algorithms for Construction and Analysis of Systems*, pages 408–426, 2018.
- [33] Xiaowei Huang, Marta Kwiatkowska, Sen Wang, and Min Wu. Safety verification of deep neural networks. In *International Conference on Computer Aided Verification*, pages 3–29, 2017.
- [34] Wenjie Ruan, Xiaowei Huang, and Marta Kwiatkowska. Reachability analysis of deep neural networks with provable guarantees. In *International Joint Conference on Artificial Intelligence*, pages 2651–2659, 2018.
- [35] Nicholas Carlini and David A. Wagner. Towards evaluating the robustness of neural networks. In *IEEE Symposium on Security and Privacy*, pages 39–57, 2017.
- [36] Osbert Bastani, Yani Ioannou, Leonidas Lampropoulos, Dimitrios Vytiniotis, Aditya V. Nori, and Antonio Criminisi. Measuring neural net robustness with constraints. In *Annual Conference on Neural Information Processing Systems*, pages 2613–2621, 2016.
- [37] Krishnamurthy Dvijotham, Robert Stanforth, Sven Gowal, Timothy A. Mann, and Pushmeet Kohli. A dual approach to scalable verification of deep networks. In *International Conference on Uncertainty in Artificial Intelligence*, pages 550–559, 2018.
- [38] Rüdiger Ehlers. Formal verification of piece-wise linear feed-forward neural networks. In *Automated Technology for Verification and Analysis - 15th International Symposium, ATVA 2017, Pune, India, October 3-6, 2017, Proceedings*, pages 269–286, 2017.
- [39] Guy Katz, Clark W. Barrett, David L. Dill, Kyle Julian, and Mykel J. Kochenderfer. Reluplex: An efficient SMT solver for verifying deep neural networks. In *International Conference on Computer Aided Verification*, pages 97–117, 2017.
- [40] Guy Katz, Derek A. Huang, Duligur Ibeling, Kyle Julian, Christopher Lazarus, Rachel Lim, Parth Shah, Shantanu Thakoor, Haoze Wu, Aleksandar Zeljic, David L. Dill, Mykel J. Kochenderfer, and Clark W. Barrett. The Marabou framework for verification and analysis of deep neural networks. In *International Conference on Computer Aided Verification*, pages 443–452, 2019.
- [41] Gagandeep Singh, Timon Gehr, Markus Püschel, and Martin T. Vechev. Boosting robustness certification of neural networks. In *International Conference on Learning Representations*, 2019.
- [42] Shiqi Wang, Kexin Pei, Justin Whitehouse, Junfeng Yang, and Suman Jana. Formal security analysis of neural networks using symbolic intervals. In *USENIX Security Symposium*, pages 1599–1614, 2018.
- [43] Shiqi Wang, Kexin Pei, Justin Whitehouse, Junfeng Yang, and Suman Jana. Efficient formal safety analysis of neural networks. In *Annual Conference on Neural Information Processing Systems*, pages 6369–6379, 2018.
- [44] Timon Gehr, Matthew Mirman, Dana Drachler-Cohen, Petar Tsankov, Swarat Chaudhuri, and Martin T. Vechev. AI2: safety and robustness certification of neural networks with abstract interpretation. In *IEEE Symposium on Security and Privacy*, pages 3–18, 2018.
- [45] Tsui-Wei Weng, Huan Zhang, Hongge Chen, Zhao Song, Cho-Jui Hsieh, Luca Daniel, Duane S. Boning, and Inderjit S. Dhillon. Towards fast computation of certified robustness for relu networks. In *International Conference on Machine Learning*, pages 5273–5282, 2018.
- [46] Patrick Cousot and Radhia Cousot. Abstract interpretation: A unified lattice model for static analysis of programs by construction or approximation of fixpoints. In *ACM SIGACT-SIGPLAN Symposium on Principles of Programming Languages*, pages 238–252, 1977.
- [47] Ramon E Moore, R Baker Kearfott, and Michael J Cloud. *Introduction to interval analysis*, volume 110. Siam, 2009.
- [48] Khalil Ghorbal, Eric Goubault, and Sylvie Putot. The zonotope abstract domain taylor1+. In *International Conference on Computer Aided Verification*, pages 627–633. Springer, 2009.
- [49] Patrick Cousot and Nicolas Halbwachs. Automatic discovery of linear restraints among variables of a program. In *ACM SIGACT-SIGPLAN Symposium on Principles of Programming Languages*, pages 84–96, 1978.
- [50] Aditi Raghunathan, Jacob Steinhardt, and Percy Liang. Certified defenses against adversarial examples. In *International Conference on Learning Representations*, 2018.
- [51] Eric Wong and J. Zico Kolter. Provable defenses against adversarial examples via the convex outer adversarial polytope. In *International Conference on Machine Learning*, pages 5283–5292, 2018.
- [52] Aleksander Madry, Aleksandar Makelov, Ludwig Schmidt, Dimitris Tsipras, and Adrian Vladu. Towards deep learning models resistant to adversarial attacks. *International Conference on Learning Representations*, 2018.
- [53] Marc Fischer, Mislav Balunovic, Dana Drachler-Cohen, Timon Gehr, Ce Zhang, and Martin T. Vechev. DL2: training and querying neural networks with logic. In *International Conference on Machine Learning*, pages 1931–1941, 2019.
- [54] Matthew Mirman, Timon Gehr, and Martin T. Vechev. Differentiable abstract interpretation for provably robust neural networks. In *International Conference on Machine Learning*, pages 3575–3583, 2018.

Appendix

7.1 Many-to-one vanilla RNN

Fig. 6 describes the structure of a many-to-one vanilla RNN. It consists of a single hidden layer, and at each time step t operates on input $\mathbf{x}(t)$ and computes the output $\mathbf{h}(t)$. At time T , it produces the output $\mathbf{y}(T) = W_{hy} \cdot \mathbf{h}(T) + \mathbf{b}_y$.

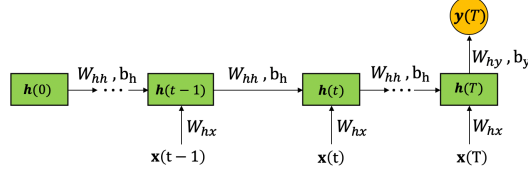


Figure 6: A many-to-one Vanilla RNN

7.2 Algorithm for differential verification of LSTMs

This appendix provides the algorithm for differential verification of LSTMs (Algo. 3), and describes the nonlinear transformer for LSTMs in Algo. 4.

Algorithm 3: Differential verification of LSTMs.

Input: network f , network f' , input region X

Output: δ^y

```

1 Init: Initialize  $[L(\mathbf{h}(0)), U(\mathbf{h}(0))]$  and  $[\underline{\delta}^h(0), \overline{\delta}^h(0)]$  to 0
2 for  $t : 1$  to  $T$  do
    // affine transformer
    // symbolic values
3   Compute  $[L(\mathbf{i}_{in}(t)), U(\mathbf{i}_{in}(t))]$ ;
4   Compute  $[L(\mathbf{f}_{in}(t)), U(\mathbf{f}_{in}(t))]$ ;
5   Compute  $[L(\mathbf{g}_{in}(t)), U(\mathbf{g}_{in}(t))]$ ;
6   Compute  $[L(\mathbf{o}_{in}(t)), U(\mathbf{o}_{in}(t))]$ ;
    // concrete differences
7   Compute  $[\underline{\delta}^i(t), \overline{\delta}^i(t)]$ ;
8   Compute  $[\underline{\delta}^f(t), \overline{\delta}^f(t)]$ ;
9   Compute  $[\underline{\delta}^g(t), \overline{\delta}^g(t)]$ ;
10  Compute  $[\underline{\delta}^o(t), \overline{\delta}^o(t)]$ ;
    // nonlinear transformer (Algo. 4)
11  Compute  $[L(\mathbf{h}(t)), U(\mathbf{h}(t))]$ ; // POPQRN
12  Compute  $[\underline{\delta}^h(t), \overline{\delta}^h(t)]$ ; // DIFFRNN
13 Compute  $[\underline{\delta}^y(T), \overline{\delta}^y(T)]$ ; // final difference interval

```

Algorithm 4: Nonlinear Transformer for LSTMs.**Input:** value intervals $\mathbf{i}_{in}(t)$, $\mathbf{f}_{in}(t)$, $\mathbf{g}_{in}(t)$, $\mathbf{o}_{in}(t)$, difference intervals $\delta_{in}^i(t)$, $\delta_{in}^f(t)$, $\delta_{in}^g(t)$, $\delta_{in}^o(t)$, $adjust=0.01$ **Output:** value $[L(\mathbf{h}(t)), U(\mathbf{h}(t))]$, difference $[\underline{\delta}^h(t), \overline{\delta}^h(t)]$

```

1 Compute  $[L(\mathbf{c}(t)), U(\mathbf{c}(t))]$ ; // POPQORN
2 Compute  $\overline{\delta}_1^c(t) = \max[\delta_1^c(t)]$ ; // global optimizer
  // dReal validation
3  $sat = dReal.CheckSat(\overline{\delta}_1^c(t) < \delta_1^c(t))$ ;
4 while  $sat == True$  do
5    $\overline{\delta}_1^c(t) = \delta_1^c(t) + adjust$ ;
6    $sat = dReal.CheckSat(\overline{\delta}_1^c(t) < \delta_1^c(t))$ ;
7 Compute  $\underline{\delta}_1^c(t) = \min[\delta_1^c(t)]$ ; // global optimizer
  // dReal validation
8  $sat = dReal.CheckSat(\underline{\delta}_1^c(t) > \delta_1^c(t))$ ;
9 while  $sat == True$  do
10   $\underline{\delta}_1^c(t) = \delta_1^c(t) - adjust$ ;
11   $sat = dReal.CheckSat(\underline{\delta}_1^c(t) > \delta_1^c(t))$ ;

  // Using global optimizer and dReal validation
12 Compute  $[\underline{\delta}_2^c(t), \overline{\delta}_2^c(t)]$ ;
  // add up the computed bounds
13  $[\underline{\delta}^c(t), \overline{\delta}^c(t)] = [\underline{\delta}_1^c(t), \overline{\delta}_1^c(t)] + [\underline{\delta}_2^c(t), \overline{\delta}_2^c(t)]$ ;
14 Compute  $[L(\mathbf{h}(t)), U(\mathbf{h}(t))]$ ; // POPQORN
  // Using global optimizer and dReal validation
15 Compute  $[\underline{\delta}^h(t), \overline{\delta}^h(t)]$ ;

```
